Proceedings of Combustion Institute – Canadian Section
Spring Technical Meeting
University of Windsor
May 12-15, 2014

Effects of Distilled Water, Sodium Chloride Solution, and Hydrochloric Acid Solution on Particulate Emission of Flares

Mohsen Kazemimanesh[1], Darcy Corbin[2], Ramin Dastanpour[3], Steven N. Rogak[3], Matthew R. Johnson[2], Larry W. Kostiuk[1], Jason S. Olfert[1*]

[1] *Department of Mechanical Engineering, University of Alberta, Edmonton, AB T6G 2G8*
[2] *Department of Mechanical and Aerospace Engineering, Carleton University, Ottawa, ON K1S 5B6*
[3] *Department of Mechanical Engineering, University of British Columbia, Vancouver, BC V6T 1Z4*

Abstract

This research is an investigation into the effects of non-hydrocarbon liquids found in fracturing fluid on particulate emissions of flares. The flaring process was simulated by a pilot-scale experiment using a 50.8-mm burner with a methane-based fuel mixture representative of upstream oil and gas (UOG) flare gas. Fuel flow rates created a range of Froude and Reynolds numbers typical of UOG flares. An atomizer was used to inject liquid droplets into the fuel flow. Transmission electron micrographs showed that the flames without liquid droplets and with distilled water droplets produced typical fractal soot agglomerates. However, in the case of flames with NaCl solution droplets, NaCl cubic crystals aggregated into spherical structures that were mostly attached to soot particles (*i.e.,* internally mixed with soot particles). Particle size distributions, soot volume fractions, and mass emission factors were obtained using Scanning Mobility Particle Sizer (SMPS) and Laser-Induced Incandescence (LII). The results showed that particle number concentration depended on the liquid mass ratio. Distilled water and hydrochloric acid solution droplets decreased emission factor. Emission factors were orders of magnitude higher when NaCl solution was injected. The particle size distribution in this case was bimodal, presumably one mode for NaCl particles and the other for soot particles. In this case, LII measured significantly lower emission factor due to the insensitivity of LII to NaCl particles, but also revealed that soot emissions were suppressed in the presence of NaCl solution. Soot mass emission factor was found to remain approximately constant in the flame without liquid at various fuel flow rates. Moreover, soot emission factors obtained by SMPS and LII agreed reasonably for the flames without and with distilled water and HCl solution.

1. Introduction

In the upstream oil and gas (UOG) industry, it is common practice to burn undesired flammable gases in a flare, and it is estimated that approximately 137 – 139 billion m^3 of gas is flared (or vented) in the world annually [1,2].

Fracturing fluids are used in the UOG industry to increase the extraction from reservoirs. Fracturing fluid is injected into the wellbore to create cracks in rock layers to provide access to oil and gas reservoirs that are isolated from the well. The formulation of the fracturing fluids mostly remains proprietary, though its main constituents are water, with various additives such as sodium chloride, acids (mostly hydrochloric acid), hydrocarbons, and polymers [3-7]. The amount of chemicals (excluding water) used in hydraulic fracturing operations is significant and estimated to be 3 million m^3 between 2005 and 2009 in the United States only [7].

A possible scenario at oil-field battery sites is that droplets of fracturing fluids can enter the flare stream [8]. Analysis of the produced water following the hydraulic fracturing at two UOG sites showed that sodium chloride was the major non-hydrocarbon liquid constituent; however, other fracturing chemicals were also present [9]. The objective of the current study was to conduct pilot-scale experiments to determine emission factors, size distributions, and the morphology of particulate matter from flames with flow conditions similar to flares in the UOG industry with droplets of non-hydrocarbon liquids.

2. Experimental Setup

For the current study, a pilot-scale flare facility was used, shown schematically in Figure 1, which consisted of a burner, droplet generation system, and particle measurement suite. The burner had ports for gaseous fuels, liquids and a drain at its base. An ultrasonic atomizer (Model 06-05108) converted the liquids to droplets with a median diameter of 38 μm. The fuel flow was directed around the atomizer to help entrainment of liquid droplets. The top of the burner was a 50.8 mm diameter tube. The fuel and liquid droplets mixed in the burner before exiting. Two sets of settling screens prevented flame buffeting, while allowing combustion air through.

* Corresponding author, E-mail: jolfert@ualberta.ca

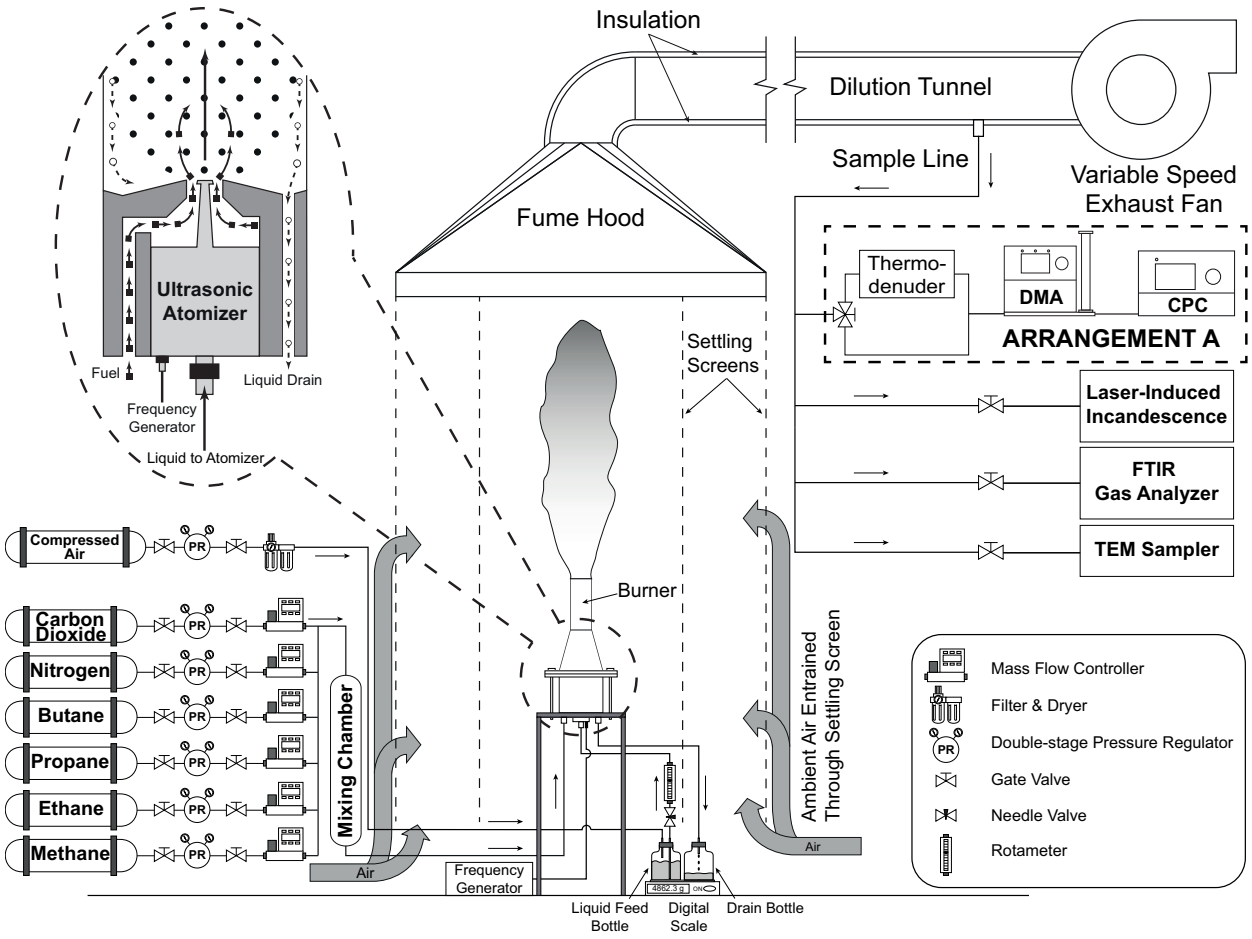

Figure 1. Schematic of the experiment setup with details of the vertical burner

Fuel mixture consisted of methane, ethane, propane, *n*-butane, carbon dioxide, and nitrogen in proportions representative of flare gas in the UOG industry [10]. The flow rate of each component was set and metered using mass flow controllers (Brooks, model 58XXS or SLA58XXS series) and mixed in a chamber prior to the burner. Five fuel flow conditions were chosen with Reynolds and Froude numbers typical of battery flares in (see Table 1).

The emission collection system consisted of a fume hood above the flame, an insulated duct, and an exhaust fan. The hood captured the entire plume of combustion products and additional entrained ambient air. The exhaust fan drew the plume into the duct and vented them to the atmosphere. Emission samples were taken from the duct via the heated sample line and directed to instrument Arrangement A, LII, and TEM sampler shown in Figure 1 (right).

Arrangement A measured particle size distribution by using an SMPS, and was comprised of a differential mobility analyzer (DMA; TSI Inc., Model 3081) and a condensation particle counter (CPC; TSI Inc., Model 3025) with settings for a measurement range of 15 – 661 nm. A thermodenuder (TD) system [11] was used upstream of the SMPS to study the volatility of particles. Particle concentrations out of the TD were corrected for diffusion and thermophoresis losses. It was found that undenuded and denuded particles had identical total concentrations and count median diameters; hence, very little semivolatile material was observed. All of the results presented in this study were reported for undenuded particles.

An LII (Artium Technologies Inc., Model LII200) was used to measure the soot volume fraction (f_v). A transmission electron microscopy (TEM) sampling unit (ESP Nano, Model 100) collected particulate matter emissions on TEM grids (NetMesh 01885-F). Samples were studied using the transmission electron microscope (Hitachi, Model H7600) operating at 80 kV. Images were taken at high resolution and magnifications in the range of 50,000 – 400,000.

Emission factor is defined as the mass of particulate matter per unit mass of fuel. To calculate emission factor, the molar flow rate in the duct must be known. The carbon conversion efficiency of the studied combustion cases were above 99.8%, therefore, assuming complete combustion and using a carbon balance, the molar flow rate of the diluted exhaust products in the duct was calculated as

Table 1. Fuel flow rate, exit velocity, source Reynolds number, and gas Froude number for the tested conditions

Fuel flow rate (SLPM)	Fuel exit velocity (m/s)	Source Reynolds number, Re_s	Gas Froude number, Fr_g
30.40	0.267	1080.1	0.00522
60.81	0.537	2160.5	0.01049
109.45	0.971	3888.6	0.01898
182.42	1.631	6480.8	0.03186
267.55	2.409	9505.2	0.04706

$$\dot{n}_{\text{duct}} = \frac{xX_{C_xH_y,\text{fuel}} + X_{CO_2,\text{fuel}} - X_{CO_2,\infty}\frac{M_{\text{fuel}}}{M_\infty} - X_{CO_2,\infty} \times 4.76\left(x+\frac{y}{4}\right)X_{C_xH_y,\text{fuel}}}{X_{CO_2,\text{duct}} - X_{CO_2,\infty}}\dot{n}_{\text{fuel}} \quad (1)$$

where $\dot{n}$ is the molar flow rate, M is the molar mass, $X_{C_xH_y,\text{fuel}}$, $X_{CO_2,\text{fuel}}$, and $X_{N_2,\text{fuel}}$ are the mole fractions of the hydrocarbon, CO_2, and N_2 in the fuel, respectively, and the subscript "∞" indicates entrained air. Parameters x and y are the number of carbon and hydrogen atoms in the hydrocarbon in the fuel, respectively. Mole fraction of CO_2 in the duct and entrained air ($X_{CO_2,\text{duct}}$ and $X_{CO_2,\infty}$, respectively) were measured by a Fourier transform infrared spectroscopy (FTIR) gas analyzer (MKS Instruments, Model Multigas 2030).

Emission factor calculated from the soot volume fraction measured by LII was

$$Y_{\text{LII}} = \frac{\dot{m}_{\text{soot}}}{\dot{m}_{\text{fuel}}} = \frac{\rho_{\text{soot}}\, f_{v,\text{LII}}\, \dot{n}_{\text{duct}}\, R\, T_{\text{LII}}}{\dot{m}_{\text{fuel}}\, P_{\text{stat}}} \quad (2)$$

where ρ_{soot} is the density of soot, $f_{v,\text{LII}}$ is the soot volume fraction measured by LII, R is the ideal gas constant, T_{LII} is the temperature of the measurement cell of LII, and P_{stat} is the static pressure in the duct measured by a pitot tube.

Similarly, mass emission factor measured by SMPS can be calculated as

$$Y_{\text{SMPS}} = \frac{(\text{mass of particles per volume of air } @T_{\text{CPC}})\, \dot{n}_{\text{duct}}\, R\, T_{\text{CPC}}}{\dot{m}_{\text{fuel}}\, P_{\text{stat}}} \quad (3)$$

where T_{CPC} is the temperature of the aerosol measurement capillary tube in the CPC, and mass of particles per volume of air is calculated by integrating the mass concentration distribution obtained from combining size distribution data with mass-mobility relationship of particles.

3. Results and Discussion

3.1 TEM analysis

TEM imaging was performed on the particulate matter samples collected from flames without and with liquid droplets at different fuel flow rates. On average 40 particles were imaged for each condition; sample images representing the majority of particles for each condition are shown if Figure 2. Figure 2(a) and 2(b) show particles from the flame with no added liquid droplets (i.e. "dry flame") and the flame with droplets of distilled water, respectively. The morphology of particles was very typical of soot generated by combustion with open, fractal-like structure. In addition to soot agglomerates, single particles were observed with ~20 nm diameters, which is typical of primary soot particles.

Figure 2(c) shows particles from the flame with droplets of NaCl solution. As illustrated, these particles are mainly composed of fractal-like soot aggregates and spherical particles containing NaCl crystals. The majority of these spherical structures, with embedded salt crystals, were attached to the soot aggregates; however, they were

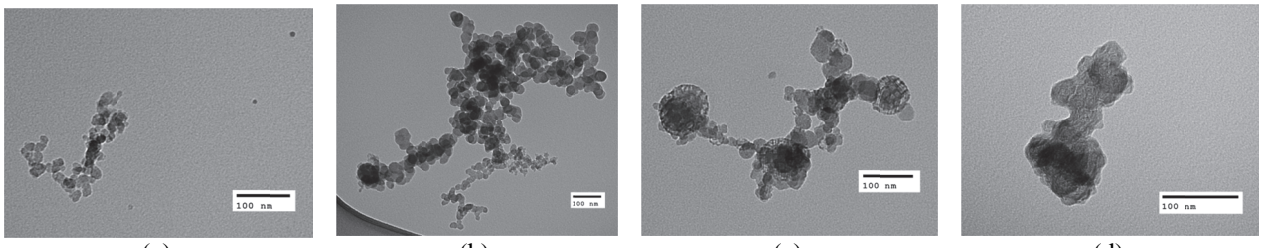

(a) (b) (c) (d)

Figure 2: TEM imaging of samples from the flame with (a) no liquid, (b) distilled water, (c) NaCl solution, and (d) HCl solution.

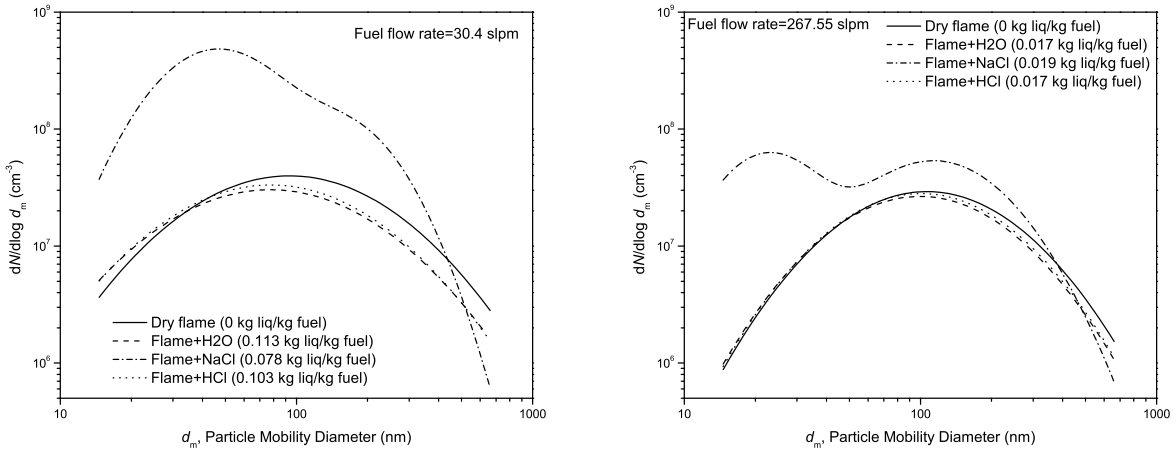

(a) (b)

Figure 3. Particle size distribution for the flare without and with different liquid droplets with (a) highest liquid mass ratio, and (b) lowest liquid mass ratio

also been observed as single particles. Typical soot agglomerates were also observed with no attached NaCl particles. These images show that NaCl particles can either be internally or externally mixed with soot aggregates in the flame with NaCl droplets.

Figure 2(d) shows particles from the flame with droplets of HCl solution. The morphology of particles was similar to a fractal-like structure in most cases; however, the primary particles were less distinguishable with the size of typical primary soot particle, but some appeared to be crumpled spheres.

3.2 Effect of liquid droplet loading on particle size distribution from flare

Figure 3 shows SMPS size distributions for particles from the flame without and with droplets of distilled water, NaCl solution, and HCl solution. The liquid droplets loading was defined as the ratio of liquid mass flow rate to fuel mass flow rate ($\dot{m}_{liquid}/\dot{m}_{fuel}$). Figure 3(a) and (b) show the size distributions for the highest and lowest liquid mass ratios, respectively.

Figure 3(a) shows that distilled water and HCl solution reduced particle concentration compared to the flare without liquid droplets, which agrees with studies that suggest that the effect of water on supressing soot is mainly due to thermal effects [12]. Distilled water and HCl solution also led to emissions of slightly smaller particles compared to the dry flame. It can be seen in Figure 3(a) that HCl solution reduced the particle concentration to a level only slightly higher than the distilled water. This result is expected as the mass of HCl solution was 99% distilled water.

Figure 3(a) also shows that the NaCl solution increased particle concentration by an order of magnitude compared to the dry flame. The size distribution was bimodal, and it is speculated that the sodium chloride is

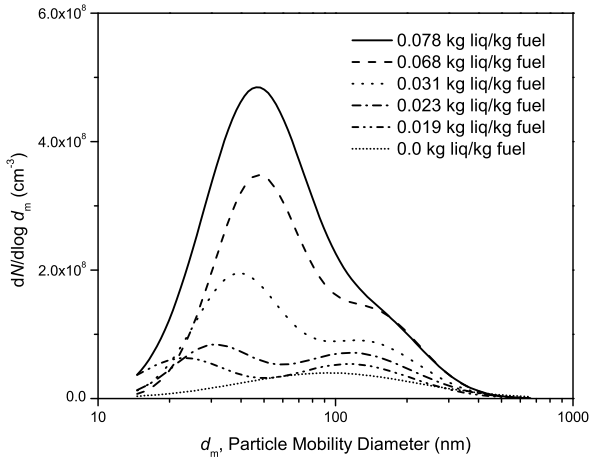

Figure 4. Particle size distribution for the flare with droplets of NaCl solution with different liquid mass ratios

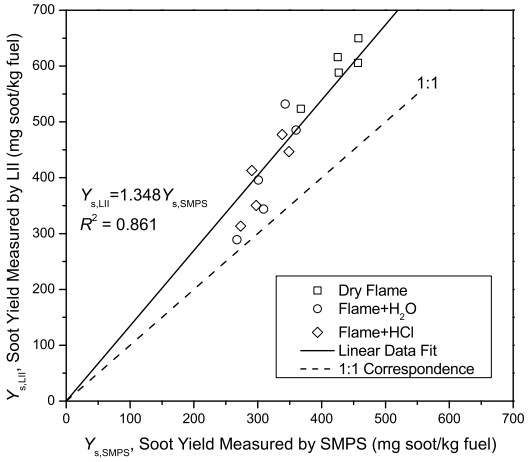

Figure 5. Comparison of soot yield measured by SMPS and LII.

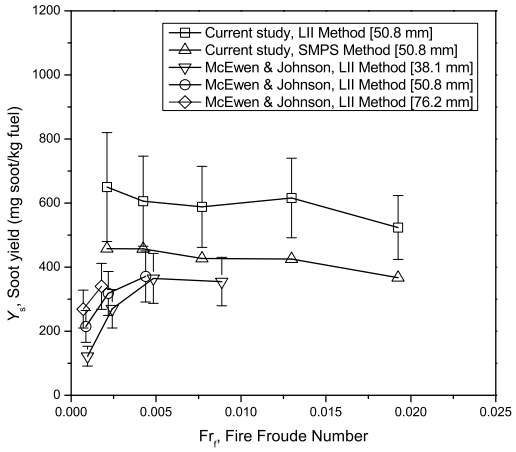

Figure 6. Soot yield as a function of fire Froude number for dry flames with the same fuel mixture composition

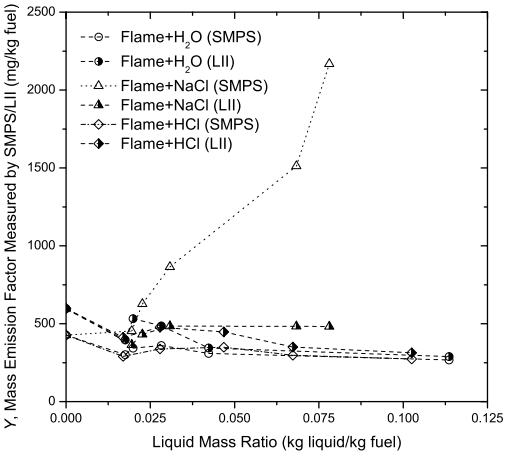

Figure 7. Particulate matter emission factor as a function of liquid mass ratio for the flame with liquid droplets

evaporated in the flame and then nucleated to generate higher number of particles with smaller size. Similar results were observed when the liquid mass ratio was lowest as in Figure 3(b); however, the effect of liquid on changing the particle concentration was less strong. In this case, all size distributions were closer to the dry flame. As all the liquid mass ratios were decreased, their corresponding particle size distributions became closer to the dry flame.

The case of flame with NaCl solution had an interesting behaviour when liquid mass ratio varied (see Figure 4). When the liquid mass ratio was highest, the size distribution was composed of a dominant first mode and a small second mode. As the liquid mass ratio was decreased, the first mode became smaller and the second mode grew larger. It is speculated that the first mode represented NaCl particles and the second mode was mostly internally-mixed soot and NaCl particles as suggested by TEM images (see Figure 2(c) and section 3.1).

Figure 5 compares soot yield measurements by SMPS and LII for flames without and with distilled water and HCl solution (flames with NaCl solution were not included as the LII did not measure NaCl particles). The linear data fit in Figure 5 shows that the LII measured ~35% higher soot yield on average compared to the SMPS. This is a reasonable agreement between the two measurements due to the high uncertainties involved in LII measurements.

3.3 Comparing soot yield results from dry flame with previous studies

Figure 6 shows the comparison of soot yield from the dry flames measured by LII and SMPS in the current study with those reported by McEwen and Johnson [10]. To scale particle emissions with the fuel flow conditions, they used the dimensionless fire Froude number defined as

$$\mathrm{Fr_f} = \frac{u_\mathrm{e} f_\mathrm{s}^{3/2}}{\left(\frac{\Delta T_\mathrm{f}}{T_\infty} g d_\mathrm{e}\right)^{1/2} \left(\frac{\rho_\mathrm{e}}{\rho_\infty}\right)^{1/4}} \tag{4}$$

where u_e is the fuel gas exit velocity, d_e is the burner exit diameter, ρ_e and ρ_∞ are the fuel and ambient air density, respectively, f_s is the stoichiometric mixture fraction, g is the gravitational acceleration, $\Delta T_\mathrm{f} = T_\mathrm{adb} - T_\infty$ is the adiabatic flame temperature (T_adb)minus the ambient temperature (T_∞).

Figure 6 shows that, in this study, with increasing fire Froude number the soot yield decreased for LII measurements but was constant for SMPS measurements; however, in [10] this trend was increasing for all three burner sizes. At large fire Froude numbers, their measured soot yields agreed well with soot yields measured by SMPS considering the uncertainties involved. The soot yield measured by SMPS had an average value of 427 mg soot/kg fuel.

3.4 Effect of liquid mass ratio on mass emission factor

Figure 7 shows the emission factors measured by SMPS and LII as a function of liquid mass ratio. The average emission factors for the dry flame measured by SMPS and LII were 427 and 597 mg soot/kg fuel, respectively. When distilled water or HCl solution were added, the SMPS- and LII-measured emission factor generally decreased compared to that of the dry flame. This result shows that water acted as a suppressant for soot production. Similar

effect from distilled water on impairing soot emissions from diffusion flames was reported in [12,13]. The HCl solution used in this study was 99% distilled water by mass; therefore, similar soot suppressing effect was expected.

When NaCl solution was injected, the emission factor measured by SMPS elevated to ~5 times of the average emission factor of the dry flame. On the other hand, the emission factor measured by LII was significantly lower than that of SMPS. The higher emission factor measured by SMPS is due to a species of particles other than soot to which the LII is insensitive. It is speculated that these are newly-formed NaCl particles in the flame based on the results of TEM imaging (section 3.1) and particle size distribution measurements (section 3.2). Figure 7 also shows that the soot yield with NaCl droplets was lower than from the dry flame. This result showed that soot formation is suppressed in the presence of NaCl droplets, which agrees with other studies that suggested alkali salts have a suppressing effect on soot produced by diffusion flames [14-16]. The particulate matter emissions in this case were consisted of two species, *i.e.,* NaCl particles and soot particles.

4. Summary

The results presented suggest that the effects of non-hydrocarbon liquids on particle emissions from flares could be significant. This exploratory study implied that NaCl solution suppressed soot formation in the flares, while significantly large numbers of NaCl particles were formed. Distilled water and very dilute HCl solution impaired soot formation. The next steps in this study would be quantification of mixing state of soot and NaCl particles. Furthermore, liquid mass ratios representative of in-situ operations will be studied. Morphology and chemical composition of particles from the flare with HCl droplets need to be addressed in future studies as well.

References

[1] U.S. Energy Information Administration, International Energy Statistics: Natural Gas Production, 2013.

[2] C.D. Elvidge, D. Ziskin, K.E. Baugh, B.T. Tuttle, T. Ghosh, D.W. Pack, E.H. Erwin, M. Zhizhin, A Fifteen Year Record of Global Natural Gas Flaring Derived from Satellite Data, Energies. 2 (2009) 595-622.

[3] U.S. Environmental Protection Agency, Evaluation of Impacts to Underground Sources of Drinking Water by Hydraulic Fracturing of Coalbed Methane Reservoirs, Report No. EPA/816/R-04/003, U.S. Environmental Protection Agency, Washington, DC, 2004.

[4] J.D. Arthur, B. Bohm, M. Layne, Hydraulic Fracturing Considerations for Natural Gas Wells of the Marcellus Shale, Paper presented at the Ground Water Protection Council Annual Forum, Cincinnati, OH, 2008.

[5] A.M. Gomaa, M.A. Mahmoud, H.A. Nasr-El-Din, Effect of shear rate on the propagation of polymer-based in-situ-gelled acids inside carbonate cores, SPE Production and Operations. 26 (2011) 41-54.

[6] New York State Department of Environmental Conservation, Revised Draft Supplemental Generic Environmental Impact Statement on the Oil, Gas and Solution Mining Regulatory Program, New York State Department of Environmental Conservation, 2011.

[7] H.A. Waxman, E.J. Markey, D. DeGette, Chemicals used in hydraulic fracturing, United States House of Representatives, Committee on Energy and Commerce, 2011.

[8] M.T. Strosher, Characterization of emissions from diffusion flare systems, Journal of the Air and Waste Management Association. 50 (2000) 1723-1733.

[9] D. McElreath, Comparison of Hydraulic Fracture Fluid Composition with Produced Formation Water Quality Following Fracturing: Implications for Fate and Transport, U.S. Environmental Protection Agency, Oklahoma City, OK, 2010.

[10] J.D.N. McEwen, M.R. Johnson, Black carbon particulate matter emission factors for buoyancy-driven associated gas flares, Journal of the Air and Waste Management Association. 62 (2012) 307-321.

[11] R. Ghazi, J.S. Olfert, Coating mass dependence of soot aggregate restructuring due to coatings of oleic acid and dioctyl sebacate, Aerosol Science and Technology. 47 (2013) 192-200.

[12] K.P. Schug, Y. Manheimer-Timnat, P. Yaccarino, I. Glassman, Sooting Behaviour of Gaseous Hydrocarbon Diffusion Flames and The Influence of Additives, Combustion Sci. Technol. 22 (1980) 235-250.

[13] V.K. Rao, M.F. Bardon, The effect of water on gas phase soot formation in laminar diffusion flames, Combust. Flame. 55 (1984) 73-78.

[14] P.A. Bonczyk, In-situ optical measurement of additive effects on particulates in a sooting diffusion flame, Combust. Flame. 51 (1983) 219-229.

[15] E.M. Bulewicz, D.G. Evans, P.J. Padley, Effect of metallic additives on soot formation processes in flames, Symp Int Combust. 15 (1975) 1461-1470.

[16] B.S. Haynes, H. Jander, H.G. Wagner, The effect of metal additives on the formation of soot in premixed flames, Symp Int Combust. 17 (1979) 1365-1374.